Hindawi
Advances in Civil Engineering
Volume 2019, Article ID 7248427, 15 pages
https://doi.org/10.1155/2019/7248427

Research Article

Effect of Particle Breakage and Shape on the Mechanical Behaviors of Granular Materials

Yongxin Wang, Shengjun Shao, and Zhi Wang

Institute of Geotechnical Engineering, Xi'an University of Technology (XAUT), No. 5 South Jinhua Road, Xi'an 710048, China

Correspondence should be addressed to Shengjun Shao; sjshao@xaut.edu.cn

Received 4 July 2019; Accepted 3 September 2019; Published 27 October 2019

Academic Editor: Sanjay Nimbalkar

The particle breakage property under loading is an important factor affecting the nonlinearity of the shear strength and stress-strain curves of coarse-grained soils. The macromechanical behaviors of coarse granular materials under consolidation and drainage shearing were tested by using a large true triaxial apparatus. The particle breakage mechanism has been analyzed by the fluctuation change of stress-strain curve and particle composition change. It was shown that the particle shape is an extremely important microproperty of the influence of granular material breakage. The variation rules of the internal friction angle and interlocking strength with the index of fine-grained breakage were sorted out, and the critical particle size for measuring the two friction modes under the given gradation was determined to be 1 mm. In addition, the numerical analysis was conducted by simulating the microshape parameters of particles. The conclusion is as follows: (1) The effect of shape parameters on shear strength can be simulated using the smoothness index F_d. (2) Compared with spherical particles, irregular-shaped particles lead to a decrease in the number of strong force chains. Moreover, more coordination numbers are needed to maintain a stable configuration, and the shear strength is improved.

1. Introduction

In high rockfill dams or embankment engineering, the properties of granular materials as the main filling material are important parameters applied widely to designing and constructing. On the one hand, it is necessary to consider the size effect [1, 2] to cause the mechanics behaviors changing. On the other hand, the granular materials under medium and high confining pressuring and shearing are prone to cause the particle breakage and alter the force chain of soil skeleton during the shearing process [3, 4], even under the low confining pressures [5].

It has been demonstrated that particle breakage significantly influences the mechanical behavior and deformation behaviors of granular coarse aggregates [6–8]. Particle breakage depends on many factors such as particle shape, size and gradation, relative density, effective stress path, and particle strength [9, 10]. Many studies have been carried out based on the phenomenon of particle breakage. Several investigators [11] attempted to establish an elastoplastic constitutive model that considers the effect of energy consumption associated with particle breakage during shearing. The crushing phenomenon of coarse-grained materials was simulated using the discrete element method to verify the dependence of particle strength on the particle size by Alaei and Mahboubi [12]. Salim and Indraratna [13] introduced an equation for the rate of particle breakage during shearing into the flow criterion to develop an elastoplastic constitutive model.

Particle shape is an extremely important microproperty of granular materials, and its influence on the macroproperties of granular materials has always been a hot issue in this field [14–17]. Shinohara et al. [16] had successively studied the influence of the particle shape on the angle of internal friction by the triaxial compression test. Some researchers have studied the mechanical response of granular media using commercial numerical software to simulate different particle shapes. With advances in modern image analysis techniques and optical instruments, some scholars have begun to study particle breakage from a mesoscopic perspective. Sun et al. [17] used a 3D imaging method to improve the characterization of ballast particles. Alikaramic

et al. [18] observed the experiment by X-ray tomography and captured the process of grain breakage and shear band formation of quartz sand. Majmudar and Behringer [19] obtained contact forces using photoelastic techniques to explain shear-induced yielding and the mechanical response.

This paper is arranged as follows: first, the particle breakage rates of different particle sizes after true triaxial test are sorted out, and the relationship between shear strength parameters (internal friction angle and interlocking strength) and particle breakage rates is revealed. And the particle breakage can be macroscopically investigated considering different factors such as intermediate principle stress and initial confining pressure. Then, combined with the numerical method, the simulation of the microshape parameters of unbreakable particles is carried out. The influence of shape parameters, such as sphericity, angularity, and roughness, on the shear strength is analyzed from the point of the force chain distribution and contact state.

2. Particle Breakage

Particle breakage in rock depends on the strength of individual particles [20], the grain size distribution [21], and the stress level. The strength of individual particles is related not only to the mineral composition but also to the shape of the particle.

2.1. Microscopic Understanding of the Particle Breakage Phenomenon. The contact state between irregular particles is very complex. The morphology of particle breakage after observation (Figure 1) can roughly be divided into three categories: fracture, surface crushing, and grinding into powder. After testing, the probability of the secondary fracture (A1) of particles is relatively small, and most of the fracture particles are divided into two parts. The number B4 in the figure is the product of the surface crushing of particles, and surface crushing mainly concentrates on the edge and the corner of particles. The number C1 represents the fine particles mainly produced by the friction action between particles.

Particle shape properties [22, 23] include form, roundness, and surface texture, which can be reflected by the shape parameters of sphericity, angularity, and roughness, respectively. The interaction and fragmentation mechanism between particles are explained in Figure 2.

Under the action of external force, body 1 is in close contact with the surrounding particles. The resultant force direction of body 1 is located on the maximum stress surface, i.e., the potential fracture surface. When the force in this direction is greater than the strength of an individual particle, the particle breaks up, and new bodies 2 and 3 are formed. Therefore, the fracture and fragmentation of particles are related to the strength of individual particles. The friction between granular materials involves two intrinsically different mechanisms, i.e., surface sliding friction and interlocking friction. For body 5 and body 6, the occlusion and interlocking effect with adjacent particles is stronger, and the edges and corners are easily sheared and broken

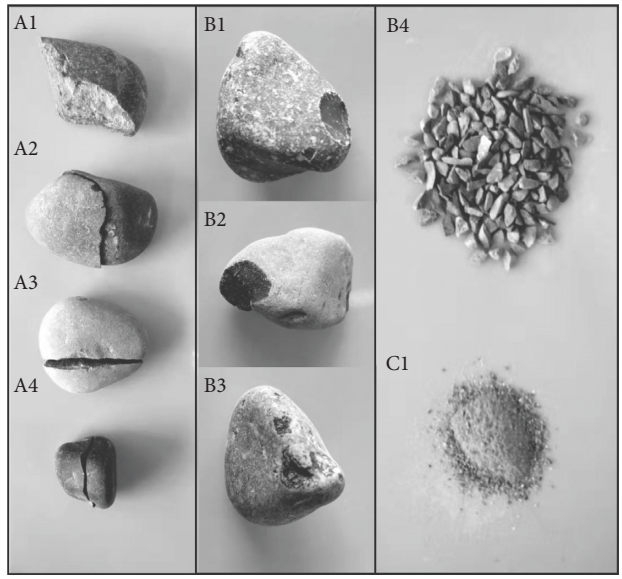

A: Fracture
B: Surface crushing
C: Powder

Figure 1: The morphology of particle breakage after testing.

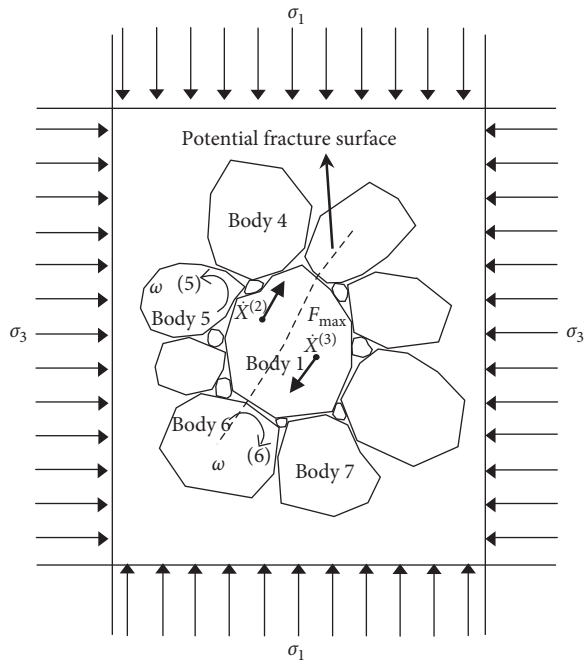

Figure 2: Mechanics mechanism of particle breakage.

during the process of particle turnover. Compared with interlocking friction, the sliding friction between particles occurs in a wider range. The rougher the surface of the particles is, the more obvious the friction and grinding effects are.

In summary, the morphology of particle breakage is related to the shape and apparent characteristics of particles. The fracture of particles is related to the strength of individual particles, which reflects the effect of mean stress. The

surface crushing and grinding of particles are mainly caused by interlocking friction and surface sliding friction, respectively. The internal relationships among the particle breakage, shape index, and mechanical properties are shown in Figure 3. The following contents mainly focus on the impact of particle breakage on the shear strength and the relationship among them through a series of experimental studies combined with numerical studies that consider the particle shape.

2.2. Influence of Particle Breakage on the Shear Strength. The irrecoverable deformation caused by particle breakage is the main reason for the nonlinear characteristics of the shear strength of coarse-grained materials. As early as 1776, Coulomb [24] presented the famous Coulomb formula (equation (1)) on the basis of experiments, which is a linear strength criterion. Obviously, at high confining pressures, the failure point does not reach the failure condition, which is not in line with the actual situation (as seen in Figure 4):

$$\tau_f = c + \sigma_f \cdot \tan\varphi, \tag{1}$$

where c is the cohesion and φ is the internal friction angle in cohesive soil, while the cohesion is nil in noncohesive soil.

Duncan et al. [26], based on conventional triaxial compression tests, proposed that the nonlinear strength parameters should take into account the characteristics that the internal friction angle of granular materials decreases with increasing confining pressure. The value of φ is the angle between the tangent of a stress circle passing through the origin and the abscissa. It can be seen that the strength curve expressed by this method is not unique:

$$\varphi = \varphi_0 - \Delta\varphi \cdot \lg\left(\frac{\sigma_3}{P_a}\right). \tag{2}$$

De Mello [27] proposed a nonlinear failure criterion for typical rockfill, where constants A and B are considered to be characteristic parameters with no obvious physical significance. The envelope corresponding to the high confining stress region clearly reveals nonlinearity:

$$\tau_f = A\sigma_n^B. \tag{3}$$

Formulas (2) and (3) are different from the Coulomb formula because they reflect the nonlinear characteristics of the shear strength of noncohesive soils. The shear strength of coarse-grained materials has obvious nonlinear characteristics, especially when particles break up at high confining pressures. This nonlinearity is because the main characteristic of coarse-grained materials is that the particle size is larger than that of fine sand and silt. Even at low confining pressures, particles are easy to break up. After particle breakage, the contact stress redistributes, and the deformation caused by particle rearrangement becomes irreversible. The more serious the particle breakage is, the more obvious the nonlinearity is.

It is generally believed that the cohesive strength of cohesionless soil does not exist [25–27]. However, a large number of engineering practices and laboratory tests have proven that cohesionless soil has interlocking strength due to the effects of interlocking and occlusion contact. The shear strength of granular soil is a comprehensive reflection of friction effect and interlocking effect. In order to facilitate understanding and engineering application, we decompose it into two parts. As seen in Figure 5, the interlocking strength is also the intercept of the tangential line of envelope at a certain confining pressure. The physical significance of parameter c is different from the cohesive strength. It can be seen that the internal friction angle is constant and the interlocking strength is close to zero for granular soil when the confining pressure is low. With an increase in the confining pressure, the internal friction angle decreases and the interlocking strength increases.

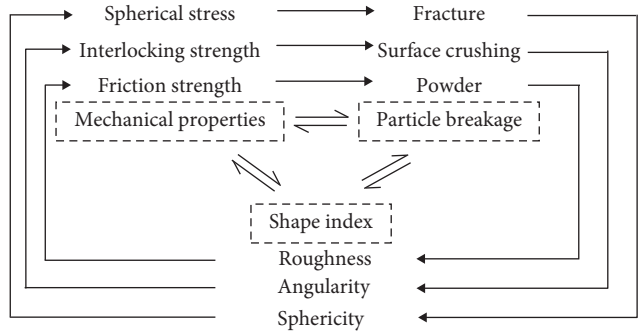

Figure 3: Relationships among particle breakage, shape index, and mechanical property.

3. Particle Breakage Tests

3.1. Testing Instrument and Material Parameters. The true triaxial apparatus used in this study, as shown in Figure 6, is a rigid-flexible-flexible boundary instrument, which was independently developed by Xi'an University of Technology. Consolidated drained triaxial tests under different stress paths were carried out on the same graded coarse-grained soil, and the particle content before and after the tests was analyzed statistically.

Coarse-grained material was taken from a river beach in Shaanxi Province (as seen in Figure 7). The ratio of length to short axis and the flatness of the selected particles meet the test requirements. The mineral composition is mainly composed of feldspar, quartz, and a small amount of mica. The particle-size distribution curve of the sample is shown in Figure 8. The size of the sample is $300 \times 300 \times 600$ mm. A series of triaxial tests were conducted with constant strain rate = 0.068%/min in the vertical direction, constant mean pressure = 200, 600 and 1000 kPa, and intermediate principal stress parameter $b = 0$, 0.25, 0.5, 0.75, and 1. Moreover, three conventional compression tests with consolidation pressures of 100, 300, and 500 kPa were also carried out.

3.2. Particle Breakage Behavior. Figure 9 shows the stress-strain curve and the local magnification diagrams in the

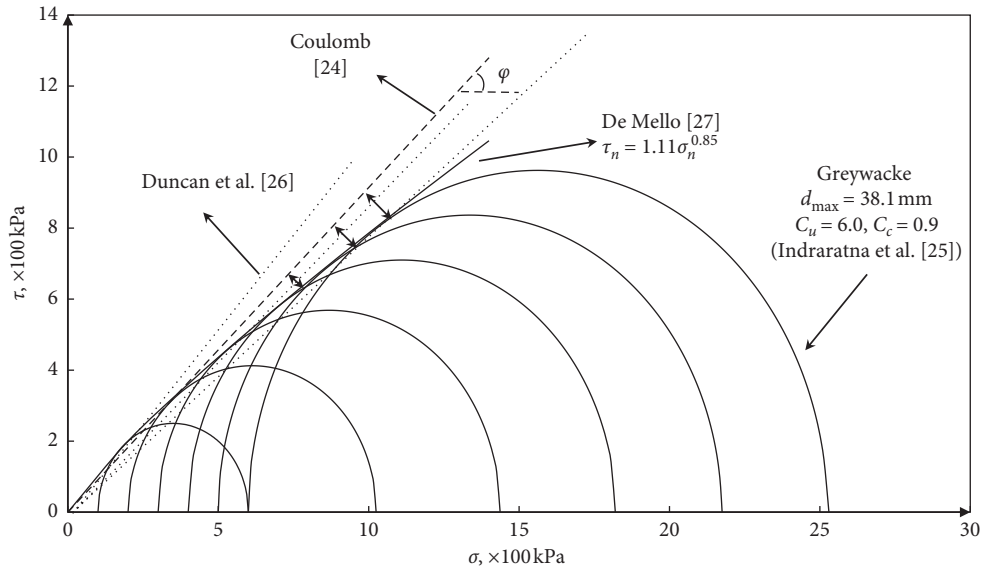

Figure 4: Several expressions of the shear strength of cohesionless soils (experimental data from Indraratna et al. [25]).

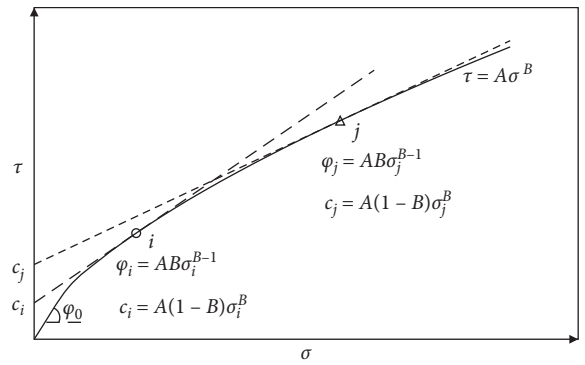

Figure 5: Calculation of interlocking strength of cohesionless soils.

shear process. There are many jumping fluctuations in the postshear curve, and the sound accompanied by particle breakage could also be heard during the test process. It indicates that particles frequently break. From an energy point of view, particle breakage is a process of energy release. Before particle breakage, energy is mainly stored in the form of elastic energy. The process of particle breakage is accompanied by the release of elastic energy, and a part of the energy consumption will be used to produce internal cracks or particle breakage.

3.3. Quantity Particle Breakage. It was found that particle breakage is unavoidable during sample preparation, consolidation stage, and shearing loading stage. To reduce the influence of particle breakage on sieving analysis during the preparation process, manual compaction was used to minimize the compaction strength. In comparison, the quantity of particle breakage in the consolidation process is much less than that in the shear process, so the effect of the shear process on particle breakage can be considered separately.

3.3.1. Sieve Analysis ($d > 2$ mm). In this paper, the particle breakage index B_g proposed by Marsal [28] is used to quantitatively describe the degree of particle breakage as a whole:

$$B_g = \sum \left|\Delta W_g\right|, \qquad \Delta W_g = W_{gi} - W_{gj}, \tag{4}$$

where W_{gi} and W_{gi} are the content of particles before and after the experiment. As shown in Figure 10, the particle breakage rate increases with increasing mean principal stress. At the same mean stress level, the particle breakage rate decreases with increasing principal stress ratio $b = (\sigma_2 - \sigma_3)/(\sigma_1 - \sigma_3)$, which is consistent with the law that the shear strength decreases with an increasing b value.

3.3.2. Sieve Analysis ($d < 2$ mm). The friction of granular materials involves two essentially different mechanisms: surface sliding friction on the contact surface and interlocking friction due to the effect of occlusal between particles. The former is related to the texture characteristics of the particle surface, and the latter is related to the angularity of the particle. The particle breakage rate B_s is defined to quantitatively describe the breakage of fine particles:

$$B_s^{i\sim j} = \frac{M_s^{i\sim j}}{M_s}, \tag{5}$$

where the molecule is the particle mass in the size interval $[i\sim j]$ and the denominator is the total particle mass with particle size less than 2 mm.

The newly generated particles ($d < 2$ mm) due to particle breakage were screened and analyzed. The results of sieve analysis for different stress paths are shown in Figure 11. The content of fine particles decreases with decreasing particle size. However, at the same value b, the change trend of fine particle content is different in

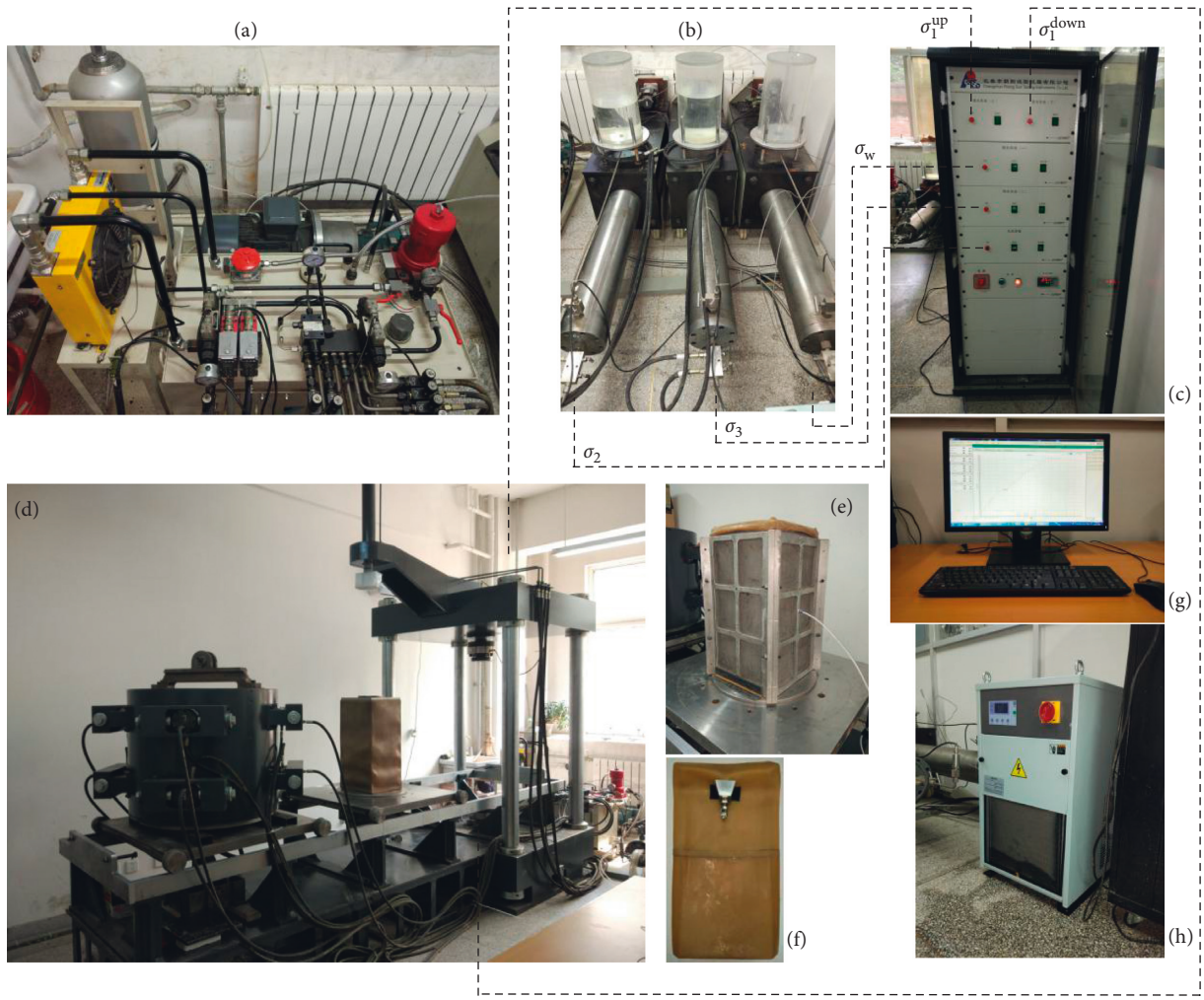

Figure 6: Physical map of a large-scale true triaxial apparatus: (a) oil source system, (b) hydraulic drive system, (c) control cabinet, (d) true triaxial mainframe, (e) specimen mold, (f) 4 flexible hydraulic rubber bags, (g) program-controlled operating interface, and (h) oil cooling system.

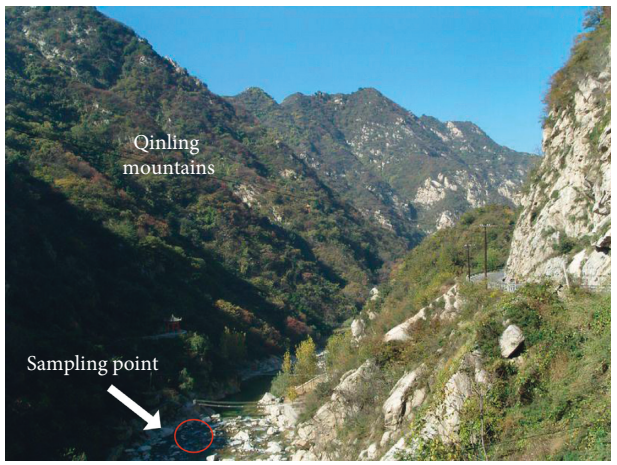

Figure 7: Location map of the sampling point.

different particle size intervals. The fine particle content increases with increasing consolidation confining pressure in particle size intervals of 1~2 mm. The particle content in other particle sizes decreases with an increase in consolidation confining pressure, and the content of particle size <0.075 mm needs to be ignored due to error of collecting.

As seen from Figure 12(a), the variation of the internal friction angle with intermediate principal stress parameter was sorted out in different mean stresses. The curves in Figure 12(b) illustrate equation (2) in terms of the relationship between the angle of internal friction $\varphi = \varphi_{13} = \sin^{-1}\{(\varphi_1 - \varphi_3)/(\varphi_1 + \varphi_3)\}$ and $\lg(p/P_a)$, indicating the effect of the mean stress p. These results show that the internal friction angle has a linear relationship with $\lg(p/P_a)$, and the shear strength represents a nonlinear characteristic.

Figure 13 shows the relationship between particle breakage index $B_s^{0\sim1}$ and internal friction angle and mean stress. It can be seen that with an increase in the mean stress, the internal friction angle decreases and the particle breakage rate decreases, which is consistent with previous understandings. At a certain mean stress level, the particle breakage rate is positively correlated with the internal friction angle, and the fitting effect is better.

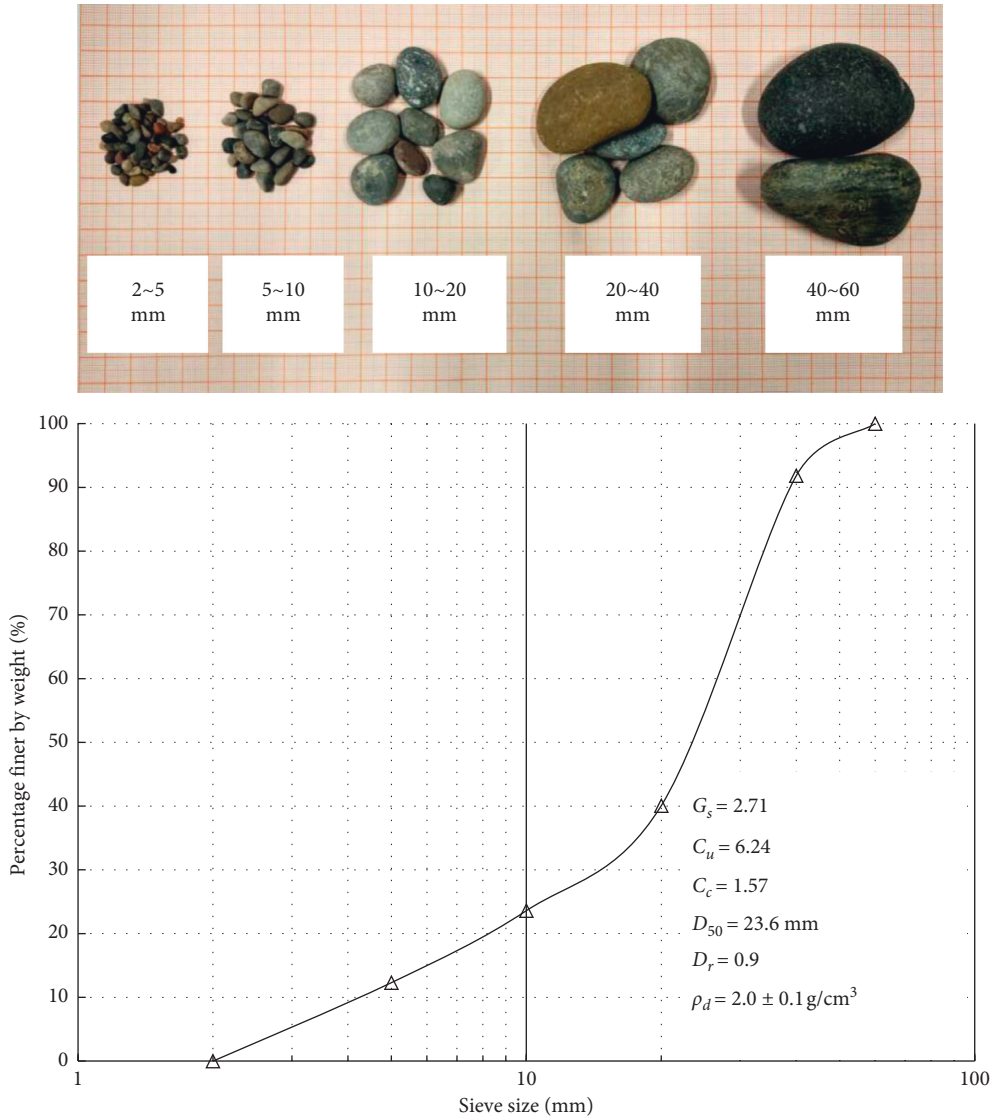

Figure 8: Grain size distribution curve.

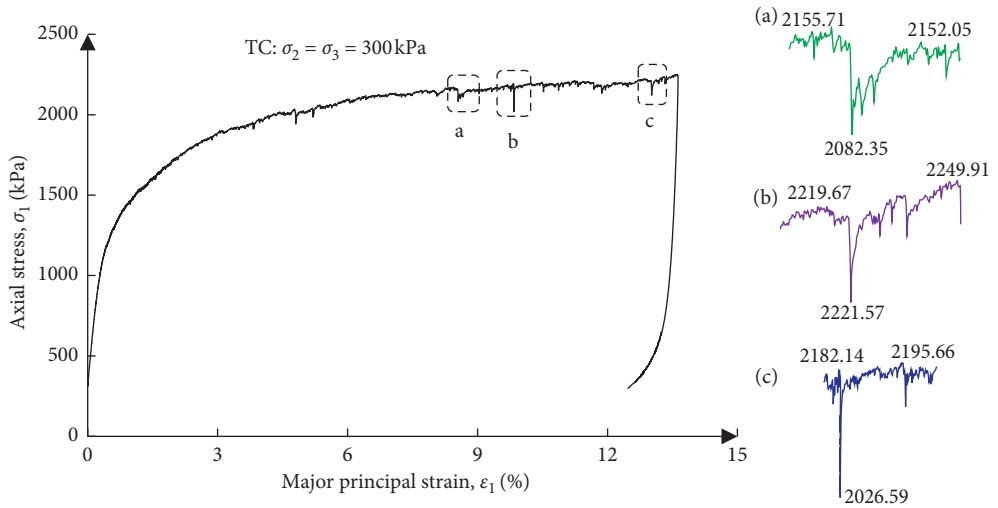

Figure 9: Fluctuation caused by particle breakage on the test curve.

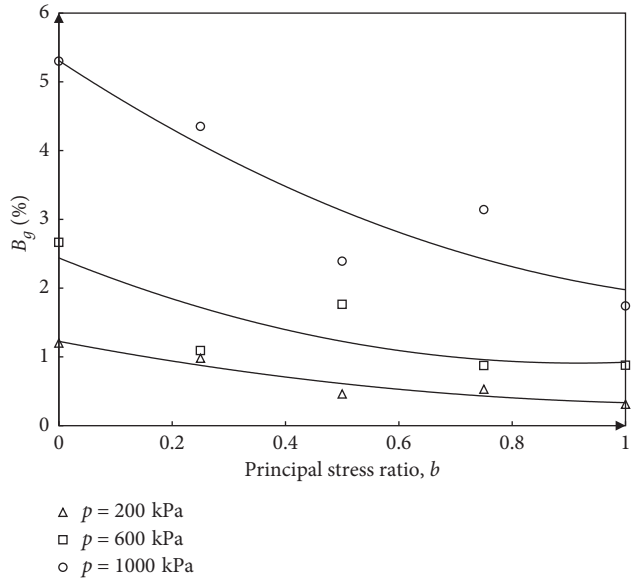

Figure 10: The relationship between the particle breakage rate and b for different mean stresses.

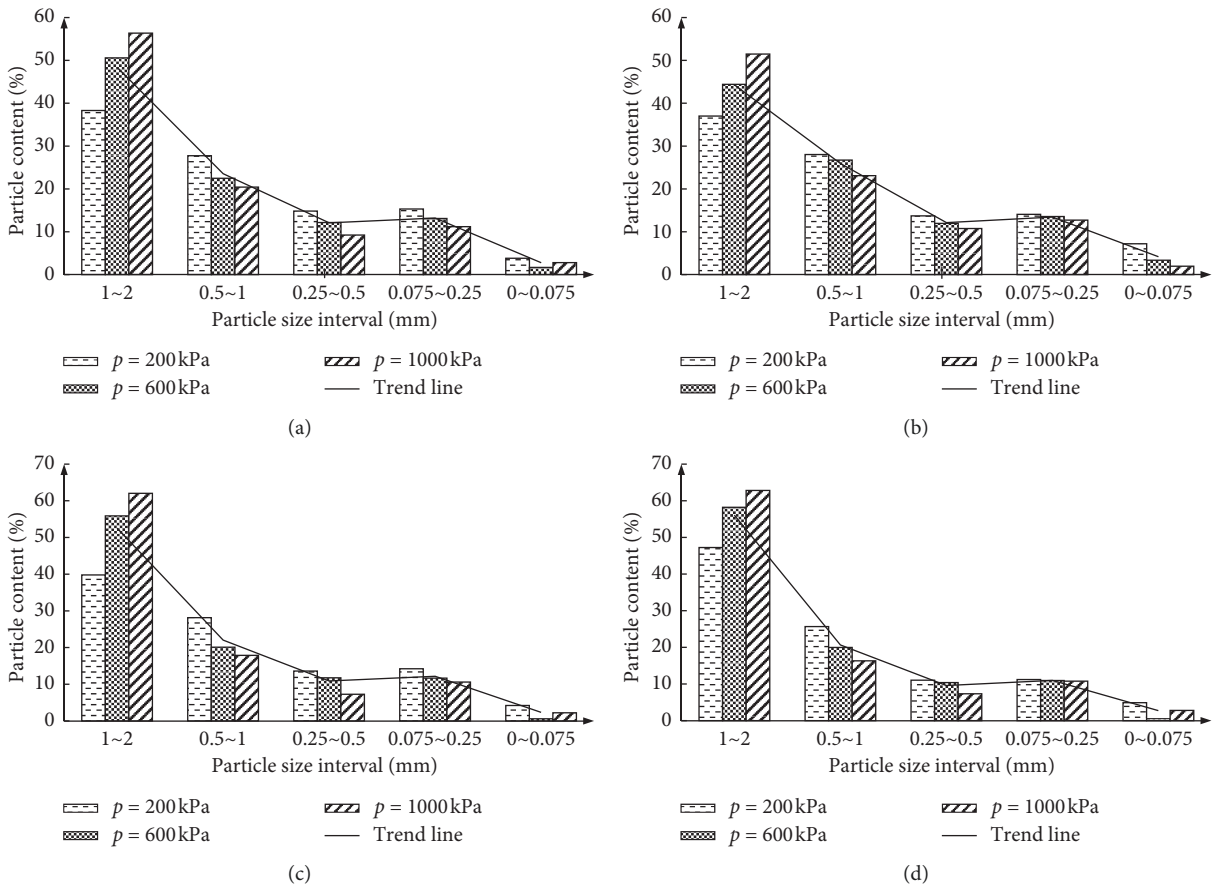

Figure 11: Continued.

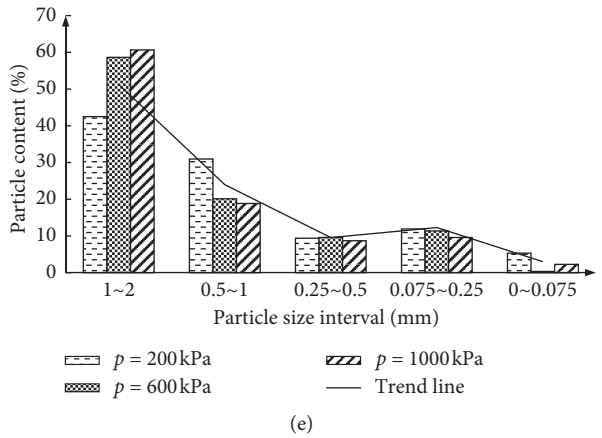

Figure 11: Sieve analysis histogram of particle breakage for different mean stresses. (a) $b = 0$, (b) $b = 0.25$, (c) $b = 0.5$, (d) $b = 0.75$, and (e) $b = 1$.

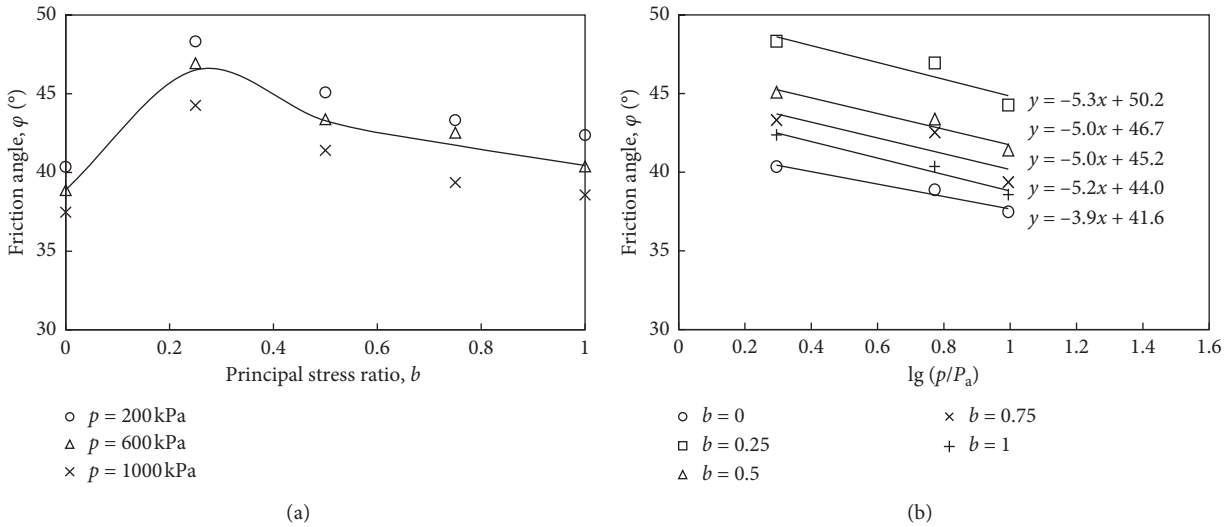

Figure 12: Relation curve between internal friction angle and mean stress for different principal stress ratios: (a) variation of the internal friction angle with intermediate principal stress ratio (b); (b) nonlinear variation of the internal friction angle with mean stress (p).

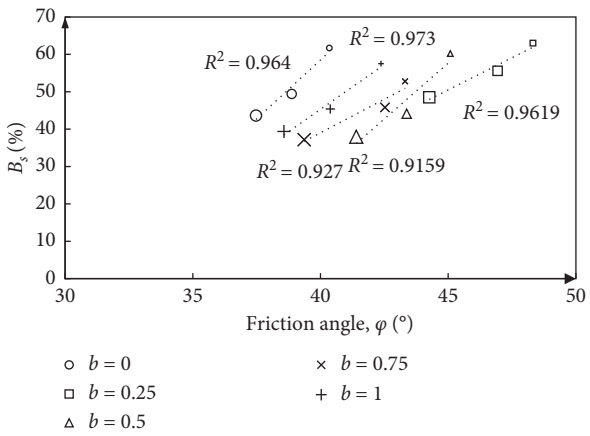

Figure 13: The relationship between particle breakage index $B_s^{0\sim1}$ and internal friction angle (the size of the marker in the figure represents the magnitude of the mean stress).

Figure 14 shows the relationship between the particle breakage index $B_s^{1\sim2}$ and interlocking strength and mean stress. The regularity of interlocking strength with an intermediate principal stress parameter is poor, especially at low mean stress. When the mean stress level is low, the intergranular biting interaction is weak, and the surface crushing is not obvious. When the mean stress $p = 1000$ kPa, the interlocking effect of particles is obviously strengthened, and the particle breakage rate increases significantly. There is a good correlation between the particle breakage index and the development of the interlocking strength. The degree of particle breakage can reflect the mechanical interlocking between particles, and the corners and surfaces of the particles are the primary places for shear breakage. Therefore, there is a certain internal relationship between the angularity, particle breakage, and interlocking strength.

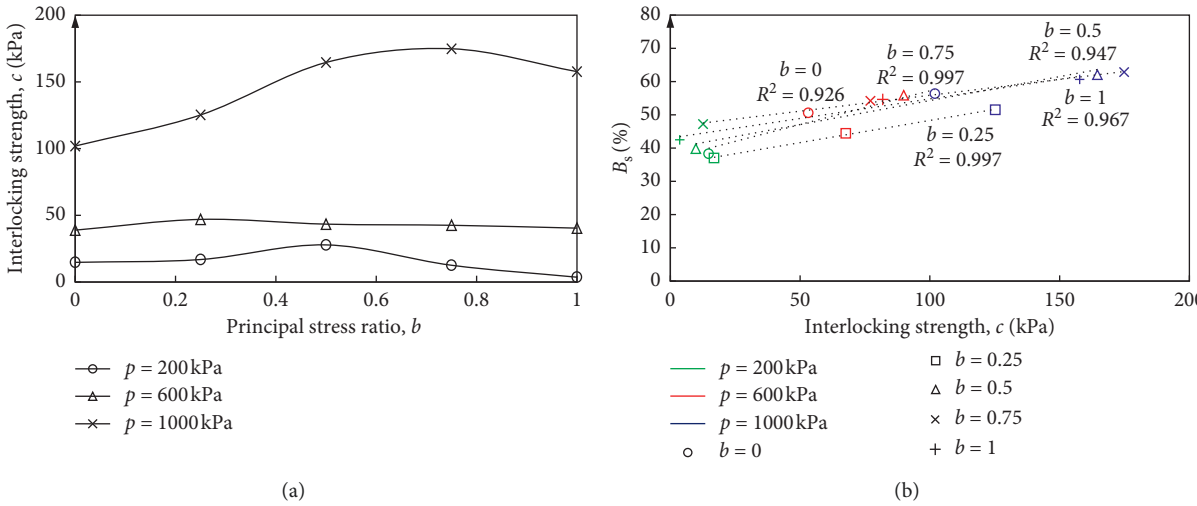

FIGURE 14: The relationship between the particle breakage index B_s and interlocking strength: (a) interlocking strength versus principal stress ratio and (b) $B_s^{1\sim2}$ versus interlocking strength.

TABLE 1: Number and shape of particles with different particle sizes.

Particle size (mm)	5~10	10~20	20~30	30~40	40~60
Particle number	4234	3961	1191	430	83
Percentage of number	42.77	40.02	12.03	4.34	0.84
Percentage of volume	3.0	22.4	21.3	37.3	16.0
Body		Ball			Clump

4. Mesoscopic Simulation of the Discrete Element Method

4.1. Construction of the Three-Dimensional Model

4.1.1. Particle Shape and Mesoscopic Parameters. The original experimental gradation is chosen as the basis of the particle-size distribution. To better consider the particle shape and improve the calculation efficiency, according to the method of equal mass substitution, particles with diameters less than 5 mm are replaced with other particle sizes.

In this paper, two kinds of solid elements are used to simulate particles: spherical particles (balls) and structural particles (clumps). The reconstruction of structural particles by using the bubble packing algorithm was proposed by Taghavi [29], in which the distance (abbreviated as F_d) is used to control the smoothness of the particle surface. F_d ranges from 0 to 180. The structural particles degenerate into spherical particles when F_d is equal to 0. On the basis of satisfying the particle profile, the larger the F_d value is, the smoother the particle surface is. The shape and quantity of particles are shown in Table 1.

To accelerate the convergence speed of the model and save the calculation time, particles with diameters less than 30 mm are simulated with spherical particles. The particles with diameters ranging from 30~60 mm are simulated using structural particles, as shown in Figure 15. The size of the sample model and particle distribution with different diameter are shown in Figure 16, and the void ratio is 0.32.

4.1.2. Contact Model. In this simulation, the influence of boundary conditions is not considered. Rigid walls are also used to simulate the lateral boundary conditions, but the mechanical parameters are slightly different. A linear contact model is used to simulate the contact constitutive relationship between particles. The contact property parameters are shown in Table 2.

4.2. Numerical Simulation Results.

The evolution of the contact force chain and contact state in the granular system plays a key role in the macroresponse of granular materials under shearing. The influence of shape parameters, such as sphericity, angularity, and roughness, on the shear strength is analyzed from the point of the force chain distribution and contact state.

4.2.1. Force Chain. Under certain boundary conditions, the fracture and reconstruction of the force chain are closely related to the shape of particles, which determines the propagation mode and shear resistance of internal forces in particles. A series of combining discrete element method (abbreviated as DEM) simulations of conventional triaxial compression tests (TC tests) with constant consolidation pressure = 100, 300, and 500 kPa were conducted.

Figure 17 shows the distribution of the three-dimensional force chain after shear failure ($\varepsilon_1 = 10\%$) of regular ($F_d = 0$) and irregular particles ($F_d = 150$). The thickness of lines representing forces is proportional to the magnitude

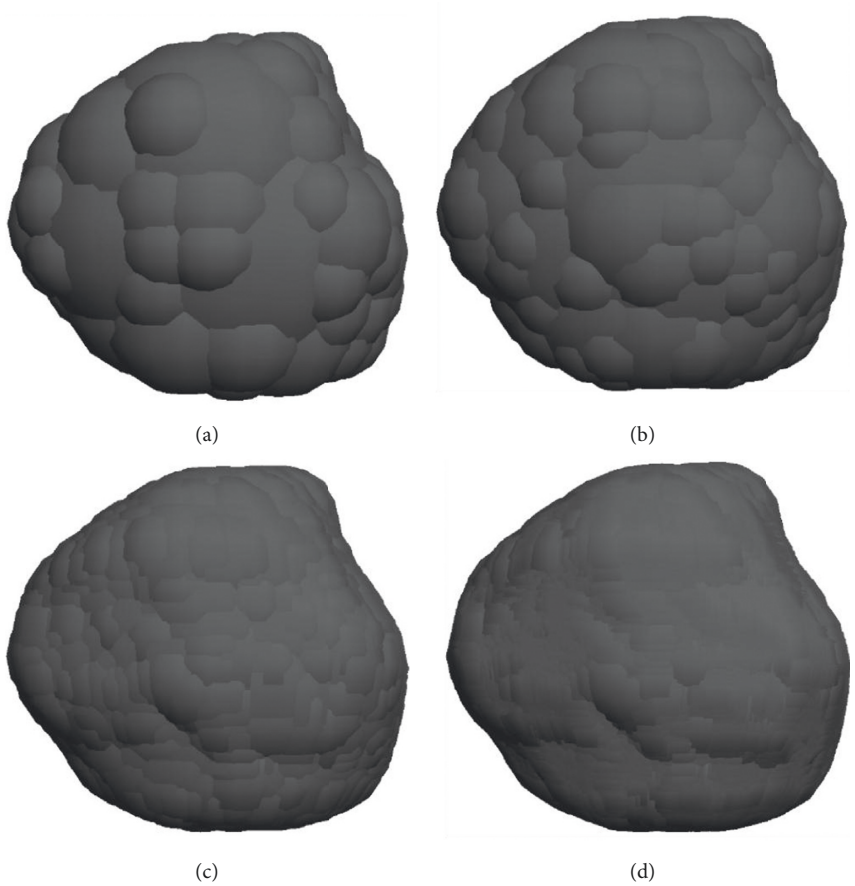

Figure 15: Construction of a three-dimensional particle model with different mesoscopic parameters. (a) $F_d = 150$, (b) $F_d = 160$, (c) $F_d = 170$, and (d) $F_d = 180$.

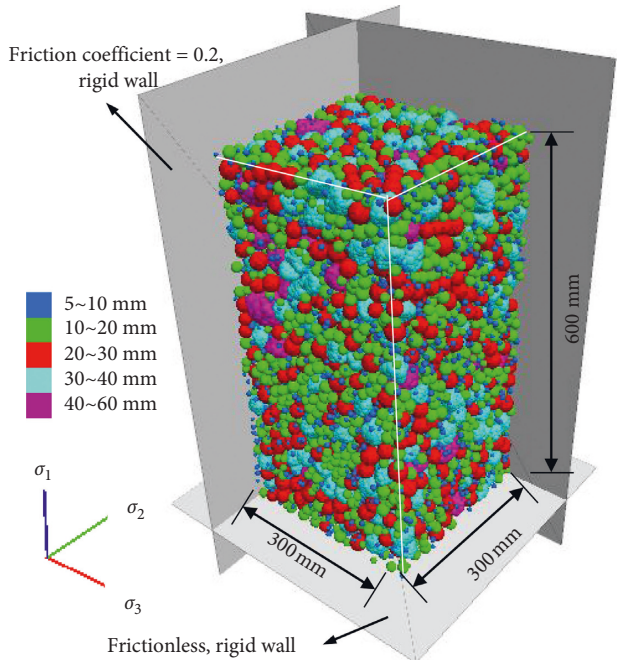

Figure 16: Three-dimensional model ($F_d = 150$).

Table 2: Contact attribute parameters of the numerical model.

Contact type		Body-body	Body-wall
Linear Contact Model	Emod, $E*$ (Pa)	1e9	1e8
	Kratio, κ	1.33	1.33
	Friction coefficient	0.3	0, 0.2 (Figure 15)
	Damping constant	0.8	—
	Particle density, ρ (kg·m^{-3})	2010	—

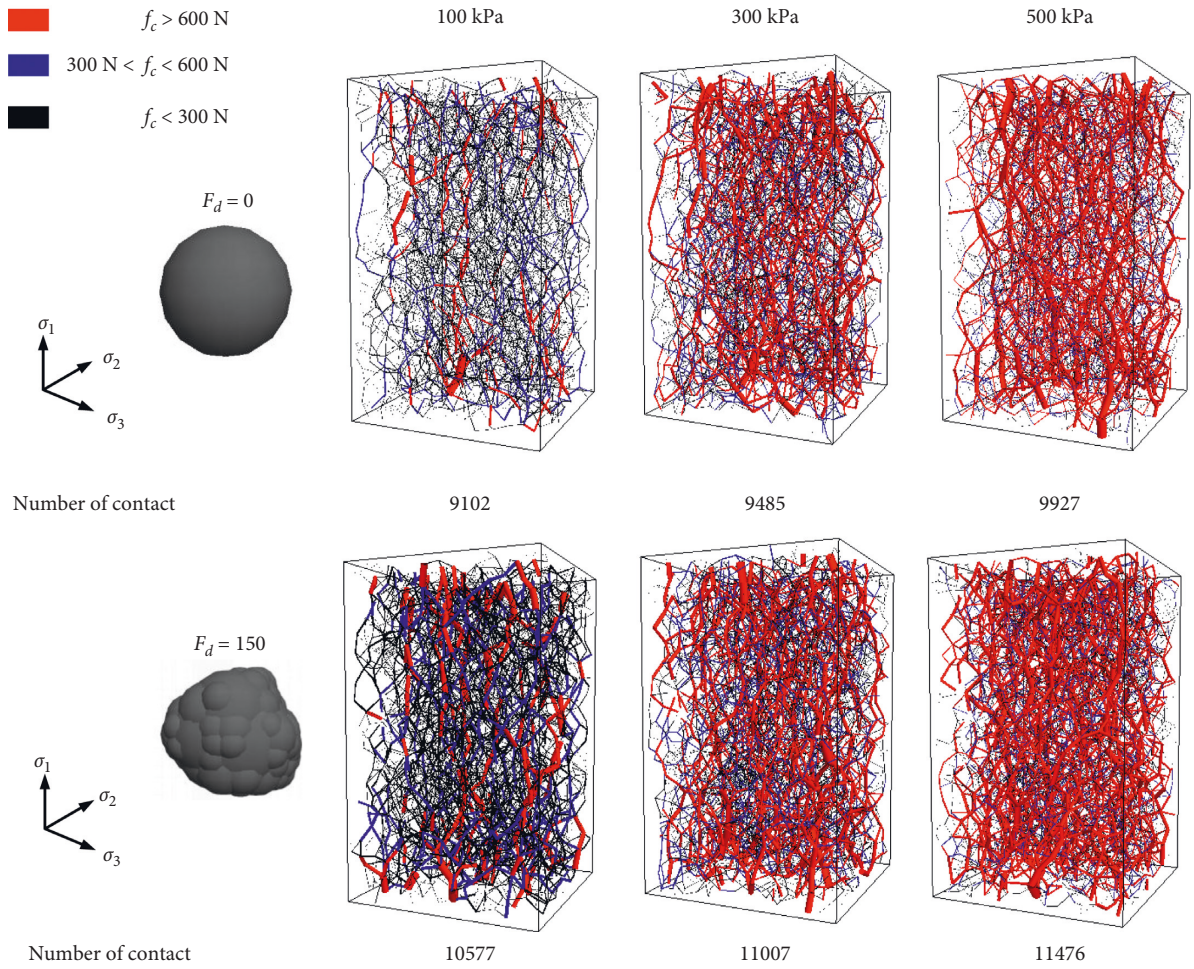

Figure 17: Three-dimensional distribution of the force chain (ε_1 = 10%).

of the contact force. The force chain with contact force less than 300 N between particles is defined as a weak force chain. The force chain with contact force greater than 600 N between particles is defined as a strong force chain. The force chain with contact force lied somewhere in between is defined as a medium force chain. Three kinds of force chains are distinguished by different colors. It can be seen that the composition of the force chain is governed by the particle-size distribution. With increasing confining pressure, the number of contacts between particles increases slightly; however, the proportion of strong force chain increases significantly. At the same confining pressure, the structural particles leads to an increase in the number of strong force chains compared to spherical particles. Moreover, the contact force of structural particles is larger than that of spherical particles. In other words, structural particles need more coordination numbers than spherical particles to maintain stable configurations.

The simulated stress-strain curves with different confining pressures are shown in Figure 18. The simulation results of regular and irregular particles can reflect the influence of the particle form on shear strength. The shear strength of irregular particles is larger than that of spherical particles, and the strength difference under high confining pressure is more obvious.

4.2.2. Contact State Analysis. During the experiment, the contact state of particles is dominated by surface sliding friction and interlocking friction. The former is related to the

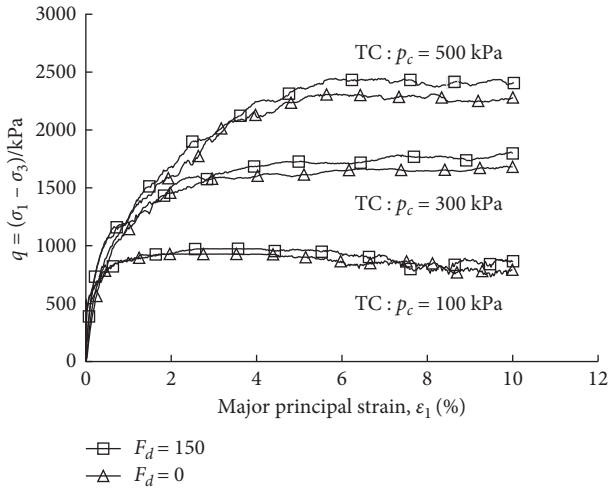

Figure 18: Effect of the particle shape on shear strength.

surface properties of the particles, and the latter is related to the angularity. To simulate the effect of the mesoshape parameters on the two modes of action, numerical simulations were carried out at confining pressures of 100, 300, and 500 kPa and F_d = 150, 160, 170, and 180, and the results were compared with those of the laboratory tests.

Figure 19 shows the relationship between the deviatoric stress and major principal strain. The numerical simulation results are basically consistent with the laboratory test results, and the softening phenomenon of the numerical simulation results is obvious at low confining pressure. Before reaching the peak strength, the stress-strain curve fluctuates greatly, and the final strength tends to be the same. At the same confining pressure, the shear strength decreases with increasing particle smoothness, but the strength difference is not obvious because the proportion of structural particles in the particle system is small.

The percentage of the locked contact can be used to measure the probability of a particle rolling in the particle system, and it also reflects the degree of angular damage of particles due to the effect of interlocking. In a DEM simulation, locked contact is governed by the Coulomb friction law. In this study, particle rolling is assumed to occur when $|f^t/(\mu \cdot f^n)| \geq 0.9999$, where f^t and f^n are the shear contact force and normal contact force, respectively, and μ is the contact friction coefficient. In general, it is assumed that some of the particles in the friction system are in the rolling state when interlocking contact is removed.

As shown in Figure 20, with an increase in axial strain, the percentage of locked contact increases rapidly until the peak value appears and then slowly decreases. In addition, the curve fluctuates frequently during the shear process, which indicates that the alternation effect of the two movement modes is significant. The same rule can also be found when combining the stress-strain curve of Figure 19. At the same confining pressure (Figure 20(a)), with a decrease in F_d, the angularity of particles is obvious, the interlocking ability with adjacent particles is strengthened, resulting in an increasing percentage of locked

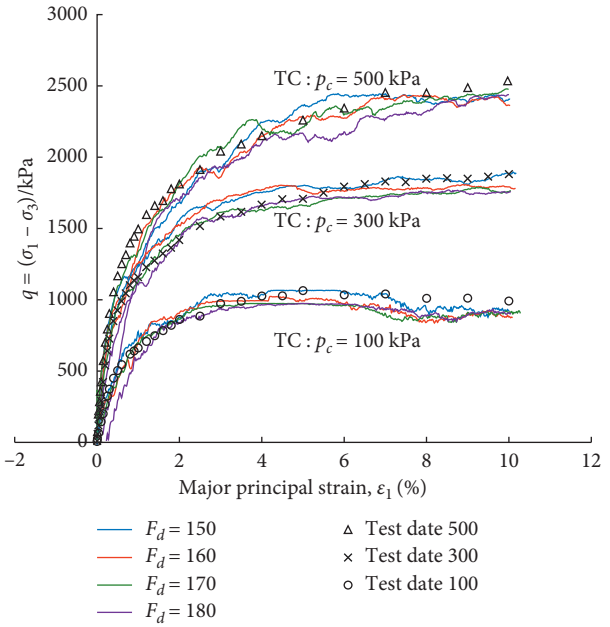

Figure 19: Effect of the particle angularity on the shear strength.

contact. At the same shape parameter (Figure 20(b)), with an increase in the confining pressure, the contact of particles becomes closer, and the percentage of locked contact increases.

In Table 3, the percentage of locked contact at peak point was statistically sorted out under several simulated working conditions. The number of total contacts is equal to the sum of the number of sliding contacts and locked contacts. With an increase in the confining pressure, the number of locked contacts increases, but the change is not obvious with varying F_d. At the same confining pressure, with a decrease in F_d, the angularity of particles is obvious, and the percentage of locked contact increases. During the process of shearing, the two friction modes coexist and can be transformed into each other. The microscopic parameters of

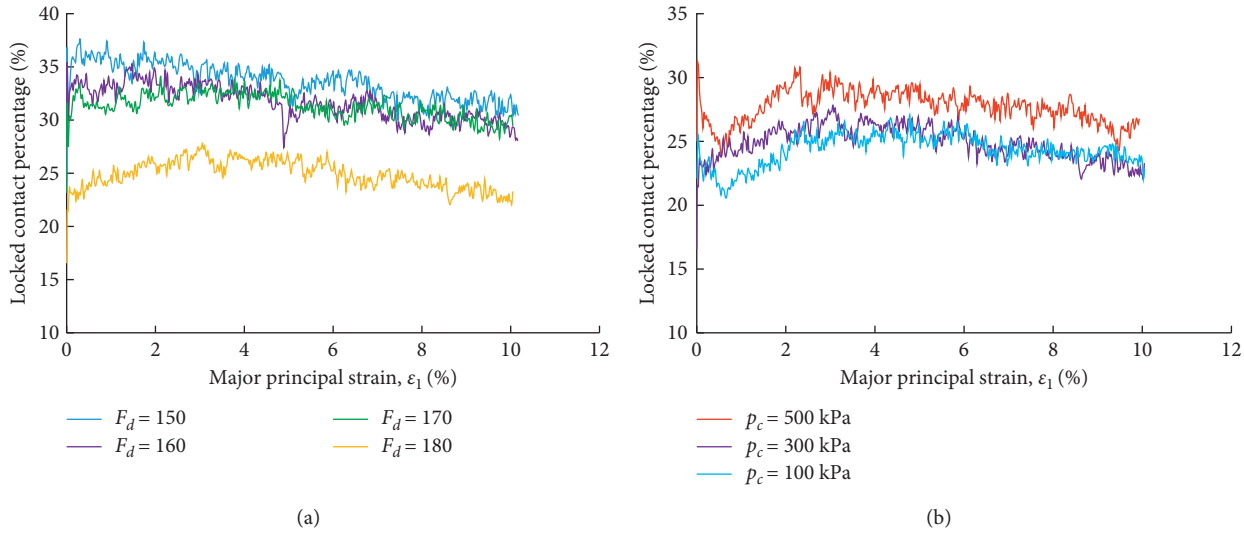

Figure 20: Variation in the locked contact percentage with major principal strain. TC tests: (a) $p_c = 300$kPa; (b) $F_d = 180$.

Table 3: Percentage of locked contact.

TC numerical simulation tests		F_d	Number of total contacts	Number of locked contacts	Locked contact percentage
p_c (kPa)	100	150	10216	3522	34.48
		160	10577	3386	32.01
		170	10794	3157	29.25
		180	13400	3589	26.78
	300	150	10829	3915	36.15
		160	11007	3920	35.61
		170	11695	3937	33.66
		180	14052	3973	28.27
	500	150	10992	4719	42.93
		160	11476	4429	38.59
		170	11878	4172	35.12
		180	14877	4600	30.92

granular materials greatly affected the macroscopic response of the granular materials.

5. Discussion

(1) The instrument used in the laboratory test is a large true triaxial apparatus with a rigid-flexible-flexible boundary. However, in the numerical simulation, the influence of boundary conditions is not considered. Whether the boundary conditions will affect the results of numerical simulation is unknown.

(2) In this paper, the critical particle size for measuring the slipping friction and interlocking friction is determined to be 1 mm, but additional experimental studies are needed to determine whether the same rule applies to other particle-size distributions.

(3) The real shape of mineral particles in rocks is quite diverse, while the shape of structural particles used in this paper is simple. In addition, the proportion of structural particles is relatively small due to the limitation of computer capacity.

6. Conclusion

(1) The mechanism of particle breakage is explained by analyzing the interaction between particles. The nonrecoverable deformation caused by particle breakage is the main reason for the nonlinear shear strength of coarse-grained materials. The morphology of particle breakage is related to the form and apparent characteristics of particles.

(2) Consolidation and drainage shear tests of coarse-grained soils with the same gradation were carried out using a large true triaxial apparatus. The variation rules of the internal friction angle and interlocking strength with the index of fine-grained breakage were sorted out, and the critical particle size for measuring the two friction modes was determined to be 1 mm to the given gradation. The sieving test shows that there

is a certain correlation between the particle breakage and the shear strength index.

(3) Particle flow software PFC3D was used to simulate the microshape parameters of the particles. The results show the following: (1) The influence of microshape parameters on the shear strength can be simulated using the smooth index F_d in the bubble packing algorithm. (2) The irregularity of particle shape leads to an increase in the number of strong force chains, the structural particles need more coordination numbers than the spherical particles to maintain stable configurations, and the shear strength is improved. (3) The shear strength decreases with increasing particle smoothness, but there is a small difference in strength due to the small proportion of structural particles in the particle system.

Data Availability

The data used to support the findings of this study are included within the article.

Conflicts of Interest

The authors declare that they have no conflicts of interest.

Acknowledgments

This paper was financially supported by the National Natural Science Foundation of China (Grant nos. 41272320 and 11572245). This support is gratefully acknowledged.

References

[1] Y. Chen, H. Liu, Y. Xiao, and W. Zhang, "Particle size effects in granular soils under true triaxial conditions," *Géotechnique*, vol. 64, no. 8, pp. 667–672, 2014.

[2] E. Frossard, W. Hu, C. Dano, and P.-Y. Hicher, "Rockfill shear strength evaluation: a rational method based on size effects," *Géotechnique*, vol. 62, no. 5, pp. 415–427, 2012.

[3] A. F. L. Nakata, M. Hyde, H. Hyodo, and Murata, "A probabilistic approach to sand particle crushing in the triaxial test," *Geotechnique*, vol. 49, no. 5, pp. 567–583, 1999.

[4] M. R. Coop, K. K. Sorensen, T. Bodas Freitas, and G. Georgoutsos, "Particle breakage during shearing of a carbonate sand," *Géotechnique*, vol. 54, no. 3, pp. 157–163, 2004.

[5] P. V. Lade, J. A. Yamamuro, and P. A. Bopp, "Significance of particle crushing in granular materials," *Journal of Geotechnical Engineering*, vol. 122, no. 4, pp. 309–316, 1996.

[6] V. Bandini and M. R. Coop, "The influence of particle breakage on the location of the critical state line of sands," *Soils and Foundations*, vol. 51, no. 4, pp. 591–600, 2011.

[7] J. de Bono and G. McDowell, "Particle breakage criteria in discrete-element modelling," *Géotechnique*, vol. 66, no. 12, pp. 1014–1027, 2016.

[8] E. Alonso, F. Iturralde, and E. Romero, "Dilatancy of coarse granular aggregates,"*Springer Proceedings in Physics,* vol. 112, pp. 119–135, Springer, Berlin, Germany, 2007.

[9] H. Shahnazari and R. Rezvani, "Effective parameters for the particle breakage of calcareous sands: an experimental study," *Engineering Geology*, vol. 159, no. 9, pp. 98–105, 2013.

[10] Y. Sun and C. Zheng, "Breakage and shape analysis of ballast aggregates with different size distributions," *Particuology*, vol. 35, pp. 84–92, 2017.

[11] B. Indraratna, S. Nimbalkar, M. Coop, and W. S. Scott, "A constitutive model for coal-fouled ballast capturing the effects of particle degradation," *Computers and Geotechnics*, vol. 61, pp. 96–107, 2014.

[12] E. Alaei and A. Mahboubi, "A discrete model for simulating shear strength and deformation behaviour of rockfill material, considering the particle breakage phenomenon," *Granular Matter*, vol. 14, no. 6, pp. 707–717, 2012.

[13] W. Salim and B. Indraratna, "A new elastoplastic constitutive model for coarse granular aggregates incorporating particle breakage," *Canadian Geotechnical Journal*, vol. 41, no. 4, pp. 657–671, 2004.

[14] A. A. Mehta and A. Patel, "An investigation on the particle breakage of Indian river sands," *Engineering Geology*, vol. 233, no. 31, pp. 23–37, 2018.

[15] J. P. de Bono and G. R. McDowell, "DEM of triaxial tests on crushable sand," *Granular Matter*, vol. 16, no. 4, pp. 551–562, 2014.

[16] K. Shinohara, M. Oida, and B. Golman, "Effect of particle shape on angle of internal friction by triaxial compression test," *Powder Technology*, vol. 107, no. 1-2, pp. 131–136, 2000.

[17] Y. Sun, B. Indraratna, and S. Nimbalkar, "Three-dimensional characterisation of particle size and shape for ballast," *Géotechnique Letters*, vol. 4, no. 3, pp. 197–202, 2014.

[18] R. Alikarami, E. Andò, M. Gkiousas-Kapnisis, A. Torabi, and G. Viggiani, "Strain localisation and grain breakage in sand under shearing at high mean stress: insights from in situ X-ray tomography," *Acta Geotechnica*, vol. 10, no. 1, pp. 15–30, 2015.

[19] T. S. Majmudar and R. P. Behringer, "Contact force measurements and stress-induced anisotropy in granular materials," *Nature*, vol. 435, no. 7045, pp. 1079–1082, 2005.

[20] G. R. McDowell and M. D. Bolton, "On the micromechanics of crushable aggregates," *Géotechnique*, vol. 48, no. 5, pp. 667–679, 1998.

[21] Y. Sun, S. Nimbalkar, and C. Chen, "Grading and frequency dependence of the resilient modulus of ballast," *Géotechnique Letters*, vol. 8, no. 4, pp. 305–309, 2018.

[22] P. J. Barrett, "The shape of rock particles, a critical review," *Sedimentology*, vol. 27, no. 3, pp. 291–303, 1980.

[23] S. J. Blott and K. Pye, "Particle shape: a review and new methods of characterization and classification," *Sedimentology*, vol. 55, no. 1, pp. 31–63, 2007.

[24] C. A. Coulomb, *Essai sur une Application des Régles de Maximis & Minimis á Quelques Problémes de Statique, Relatifs á l'Architecture, Memoires de Mathematique de l'Academie Royale de Science 7*, Paris, France, 1776.

[25] B. Indraratna, L. S. S. Wijewardena, and A. S. Balasubramaniam, "Large-scale triaxial testing of greywacke rockfill," *Géotechnique*, vol. 43, no. 1, pp. 37–51, 1993.

[26] J. M. Duncan, P. Byrne, K. S. Wong, and P. Mabry, "Strength stress-strain and bulk modulus parameters for finite element analyses of stresses and movements in soil masses," Report No. UCB/GT/80-01, Dept. of Civil Engineering, University of California, Berkeley, CA, USA, 1980.

[27] V. F. B. De Mello, "Reflection on decisions of practical significance to embankment dam constitution: 17th rankine lecture," *Geotechnique*, vol. 27, no. 3, pp. 281–355, 1977.
[28] R. J. Marsal, "Large-scale testing of rockfill materials," *Journal of the Soil Mechanics and Foundations Division*, vol. 93, no. 2, pp. 27–43, 1967.
[29] R. Taghavi, "Automatic clump generation based on mid-surface," in *Proceedings of the 2nd International FLAC/DEM Symposium*, pp. 791–797, Melbourne, Australia, February 2011.